World beyond the nearest neighbors

OPEN ACCESS
IOP Publishing
Journal of Physics: Condensed Matter
J. Phys.: Condens. Matter **35** (2023) 174002 (6pp)
https://doi.org/10.1088/1361-648X/acbe24

World beyond the nearest neighbors

Takeshi Egami[1,2,3,*] **and Chae Woo Ryu**[1,4]

[1] Shull-Wollan Center and Department of Materials Science and Engineering, University of Tennessee, Knoxville, TN 37996, United States of America
[2] Department of Physics and Astronomy, University of Tennessee, Knoxville, TN 37996, United States of America
[3] Materials Science and Technology Division, Oak Ridge National Laboratory, Oak Ridge, TN 37831, United States of America
[4] Department of Materials Science and Engineering, Hongik University, Seoul 04066, Republic of Korea

E-mail: egami@utk.edu

Received 21 November 2022, revised 31 January 2023
Accepted for publication 22 February 2023
Published 3 March 2023

Abstract
The structure beyond the nearest neighbor atoms in liquid and glass is characterized by the medium-range order (MRO). In the conventional approach, the MRO is considered to result directly from the short-range order (SRO) in the nearest neighbors. To this bottom–up approach starting with the SRO, we propose to add a top–down approach in which global collective forces drive liquid to form density waves. The two approaches are in conflict with each other, and the compromise produces the structure with the MRO. The driving force to produce density waves provides the stability and stiffness to the MRO, and controls various mechanical properties. This dual framework provides a novel perspective for description of the structure and dynamics of liquid and glass.

Keywords: liquid and glass, medium-range order, density wave, viscosity and deformation

(Some figures may appear in colour only in the online journal)

1. Introduction

Liquid is a condensed matter of which physical density is similar to that of solid. Atoms are not totally randomly distributed but are strongly correlated in space and time. To elucidate such local correlations and to relate them to the properties have long been a major challenge [1–3]. The conventional approach to elucidating the structure is to start with local structural units made of several atoms, and to use them as building blocks to form a global structure, the local *bottom–up* approach [4–7]. However, this approach fails to explain the strong drive to form the medium-range order (MRO) among atoms beyond the nearest neighbors, which is different in nature from the short-range order (SRO) among the nearest neighbors [8–11]. We propose to add a global *top-down* approach to explain the driving force to form the MRO [12, 13]. In this approach we start with a high-temperature gas state and apply interatomic potentials to all atoms at once in reciprocal space. This causes collective density wave instability in all directions with the same wavelength. These two driving forces, local and global, are in competition and are mutually frustrated. The final structure is determined through the compromise of frustration between these two, which results in the MRO. This even-handed approach on global and local structures explains the distinct natures of SRO and MRO and elucidates various properties of liquid and glass.

2. Nature of the MRO

Because liquid and glass do not have periodic structures, their structure is usually described by the atomic pair-distribution function (PDF),

* Author to whom any correspondence should be addressed.

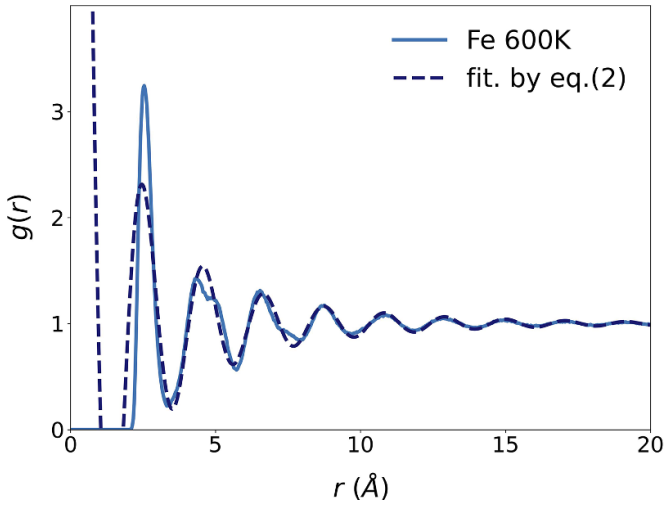

Figure 1. The PDF of supercooled liquid Fe at 600 K (solid curve), and the fit by equation (2) (dashed curve) with $Q_{\mathrm{MRO}} = 3.02$ Å^{-1}, $\delta_{MRO} = 0.227$, and $\xi_{\mathrm{s}} = 7.66$ Å.

$$g(r) = \frac{1}{4\pi N\rho_0 r^2}\sum_{i,j}\langle\delta(r - |\boldsymbol{r_i} - \boldsymbol{r_j}|)\rangle, \tag{1}$$

where $\boldsymbol{r_i}$ is the atomic position of the i-th atom, N is the number of atoms in the system, ρ_0 is the average number density of atoms, and $<\ldots.>$ denotes thermal and ensemble average [1, 3]. Whereas the PDF depicts the distribution of distances between two atoms at the same time, the information it carries is not limited strictly to the two-body correlations. For instance, its derivative catches some features of the three-body correlations. The PDF shows oscillations indicating a shell-like structure around each atom. The first peak describes the SRO in the nearest neighbor atoms, and the peaks beyond the first peak describes the MRO. As shown in figure 1 the MRO oscillations are given approximately by,

$$g(r) - 1 \approx A_{\mathrm{MRO}}\frac{a}{r}\sin(Q_{\mathrm{MRO}}r + \delta_{\mathrm{MRO}}) \times \exp\left(-\frac{r}{\xi_s}\right), \quad r > r_{\mathrm{cutoff}}, \tag{2}$$

where A_{MRO} is the amplitude of the MRO oscillation, a is the average distance to the nearest neighbors, δ_{MRO} is the phase factor which is small, ξ_{s} is the structural coherence length and r_{cutoff} is the position of the first minimum of the PDF beyond the first peak [11].

The structural coherence length, ξ_{s}, follows the Curie-Weiss law for temperature dependence above the glass transition temperature, T_{g},

$$\frac{\xi_{\mathrm{s}}(T)}{a} = C\frac{T_{\mathrm{g}}}{T - T_{\mathrm{IG}}} \quad (T > T_{\mathrm{g}}), \tag{3}$$

where T_{IG} is the ideal glass (IG) temperature at which $\xi_{\mathrm{s}}(T)$ diverges in extrapolation [9]. Below T_{g} ξ_{s} freezes at a constant value. In contrast, the SRO, described by the height of the first peak of $g(r)$, does not freeze at T_{g} and keeps increasing with decreasing temperature below T_g [11]. These different behaviors through T_{g} indicate that the MRO is not a mere consequence of the SRO, as has been assumed for a long time [14]. They represent correlations with fundamentally difference natures. The number of atoms involved in the first peak of the PDF, the coordination number N_{C}, is 12–14 for simple liquids, such as metallic liquids [2–4], and is less for covalent liquids. However, at longer distances a PDF peak covers a much larger number of neighbor atoms. The width of the higher-order peaks in the PDF is of the order of 1 Å, much wider than the typical phonon amplitudes which are of the order of 0.1 Å. Therefore, the peaks in the PDF beyond the first neighbors do not represent individual interatomic distances, but instead they describe features of more coarse-grained, local density fluctuations [10]. In other words, the first peak describes the *point-to-point* correlations, but the MRO describes the *point-to-set* correlations [15].

The structural coherence length, ξ_{s}, increases with decreasing temperature, and diverges at T_{IG}. The state with diverging ξ_{s}, the structurally coherent IG state, cannot be reached in reality, because the structure freezes at T_{g} and also T_{IG} is negative for all metallic liquids we studied [11]. However, this state, characterized by long-range density waves [9], provides an important reference point in the argument. For this state the first peak of the structure function, $S(q)$, which is the Fourier-transform of $g(r)$ [16], is a Bragg-like δ-function [9]. Then, what is driving the system toward this ideal state as temperature is reduced? We found an answer to this question through the top–down approach with the density wave theory and the novel concept of the pseudopotential for interatomic interaction.

3. Density wave theory and pseudopotential

We consider an assembly of non-interacting atoms in the high-density gas state, and introduce the interatomic potential to all atoms at once. To describe such a state, it is convenient to use the density waves in reciprocal space [16, 17]. We describe the structure in terms of local density, $\rho(\boldsymbol{r})$, and its Fourier-transform, $\rho(\boldsymbol{q})$, as

$$\rho(\boldsymbol{r}) = \sum_i \delta(\boldsymbol{r} - \boldsymbol{r_i}) = \int \rho(\boldsymbol{q})\, e^{i\boldsymbol{q}\cdot\boldsymbol{r}}\mathrm{d}\boldsymbol{q}, \tag{4}$$

$$\rho(\boldsymbol{q}) = \frac{1}{V}\int \rho(\boldsymbol{r})\, e^{-i\boldsymbol{q}\cdot\boldsymbol{r}}\mathrm{d}\boldsymbol{r}. \tag{5}$$

where V is the system volume. The $\rho(\boldsymbol{q})$ describes the density waves and is related to the structure function by diffraction, $S(\boldsymbol{q})$, through

$$S(\boldsymbol{q}) = \frac{V}{\rho_0}|\rho(\boldsymbol{q})|^2. \tag{6}$$

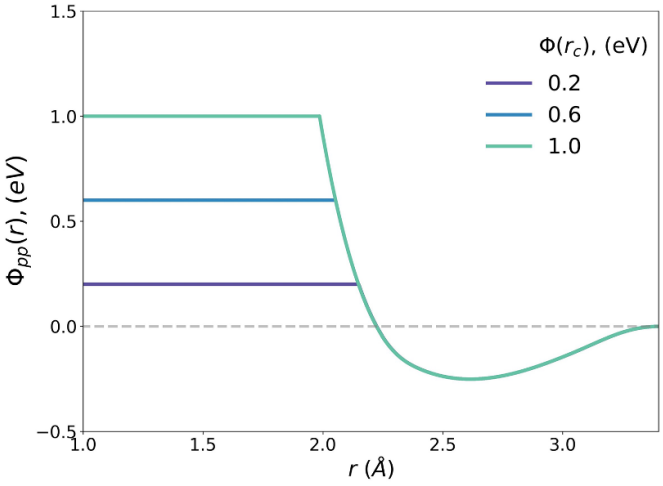

Figure 2. The pseudopotential, $\phi_{\rm pp}(r)$, for the modified Johnson potential (mJP) of Fe with various values of $\phi(r_{\rm c})$.

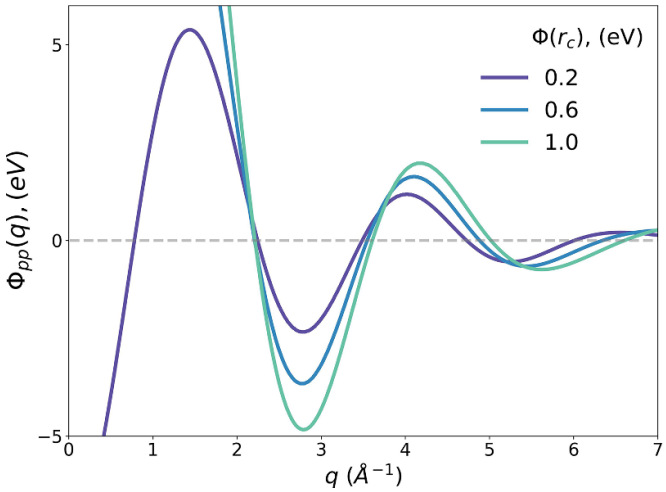

Figure 3. The $\phi(q)$ and $\phi_{\rm pp}(q)$ of Fe with various cutoff values.

For atoms interacting with a spherical interatomic potential, $\phi(r)$, the total potential energy is,

$$U=\frac{1}{V}\int\rho(\boldsymbol{r})\,\rho^{*}(\boldsymbol{r'})\,\phi(|\boldsymbol{r}-\boldsymbol{r'}|)\,\mathrm{d}\boldsymbol{r}\mathrm{d}\boldsymbol{r'}=\int|\rho(\boldsymbol{q})|^{2}\phi(|\boldsymbol{q}|)\,\mathrm{d}\boldsymbol{q}, \tag{7}$$

where

$$\phi(|\boldsymbol{q}|)=\phi(q)=\int\phi(|\boldsymbol{r}|)\,e^{-i\boldsymbol{q}\cdot\boldsymbol{r}}\mathrm{d}\boldsymbol{r}=4\pi\int\phi(r)\,\frac{\sin(qr)}{qr}r^{2}\,\mathrm{d}r. \tag{8}$$

The model, of which PDF is shown in figure 1, was calculated with modified Johnson potential (mJP) [18]. The $\phi(r)$ of the mJP has a minimum at $r_{\rm min}=2.62$ Å, which is in close vicinity to the position of the first peak of the PDF, r_1. The $\phi(q)$ is dominated by the highly repulsive part of the $\phi(r)$. However, the strongly repulsive part of the potential has no real effect on the total energy, because atoms cannot come so close to each other. For this reason, we split the potential into two parts,

$$\phi(r)=\phi_{\rm pp}(r)+\phi_{\rm R}(r). \tag{9}$$

Here $\phi_{\rm pp}(r)$ is the 'pseudopotential' in which the strongly repulsive part of $\phi(r)$ is removed and $_{\rm pp}(r)=(r_{\rm c})$ is assumed for $r<r_{\rm c}$ as shown in figure 2 [12]. The cutoff, $r_{\rm c}$, is chosen such that the cutoff temperature, $k_{\rm B}T_{\rm u}=(r_{\rm c})$ is well above the actual temperature and no pair of atoms is found at distances $r<r_{\rm c}$. The $\phi_{\rm R}(r)$ is the repulsive part of the potential below $r_{\rm c}$. Then the total potential energy is,

$$U=U_{\rm pp}+U_{\rm R}, \tag{10}$$

$$U_{\rm pp}=\frac{1}{V}\int\rho(\boldsymbol{r})\,\rho^{*}(\boldsymbol{r'})\,\phi_{\rm pp}(|\boldsymbol{r}-\boldsymbol{r'}|)\,\mathrm{d}\boldsymbol{r}\mathrm{d}\boldsymbol{r'}, \tag{11}$$

$$U_{\rm R}=\frac{1}{V}\int\rho(\boldsymbol{r})\,\rho^{*}(\boldsymbol{r'})\,\phi_{\rm R}(|\boldsymbol{r}-\boldsymbol{r'}|)\,\mathrm{d}\boldsymbol{r}\mathrm{d}\boldsymbol{r'}=0. \tag{12}$$

Note that $U_{\rm R}=0$, because no pair of atoms is found at distances at $|\boldsymbol{r}-\boldsymbol{r'}|<r_{\rm c}$, where $\phi_{\rm R}(r)$ is non-zero. Thus, we only need to minimize $U_{\rm pp}$ to determine the ground state.

Surprisingly, as shown in figure 3, $\phi_{\rm pp}(q)$, the Fourier-transform of $\phi_{\rm pp}(r)$, was found to have a strong minimum at $q_{\rm min}$, which is very close to q_1, the position of the first peak of $S(q)$. Then, the density wave state with $q_{\rm IG}=q_{\rm min}$ will minimize $U_{\rm pp}$. Because liquid is isotropic,

$$\rho_{\rm pp}(\boldsymbol{r})=\rho_{{\rm IG},\boldsymbol{\Lambda}}(\boldsymbol{r})=\rho_0+\int\rho_{\boldsymbol{\Lambda}}(\boldsymbol{q}_{\rm IG})\,e^{i\boldsymbol{q}_{\rm IG}\cdot\boldsymbol{r}}d\boldsymbol{q}_{\rm IG}, \tag{13}$$

where $|\boldsymbol{q}_{\rm IG}|=q_{\rm IG}$ form a sphere, and

$$\rho_{\boldsymbol{\Lambda}}(\boldsymbol{q}_{\rm IG})=|\rho_{\boldsymbol{\Lambda}}(\boldsymbol{q}_{\rm IG})|\,e^{i\delta_{{\rm IG},\boldsymbol{\Lambda}}(\boldsymbol{q}_{\rm IG})}. \tag{14}$$

Here Λ refers to a set of the amplitudes, $|\rho_{\boldsymbol{\Lambda}}(\boldsymbol{q}_{\rm IG})|$, and the phase factors, $\delta_{{\rm IG},\boldsymbol{\Lambda}}(\boldsymbol{q}_{\rm IG})$, within the sphere of constant $|\boldsymbol{q}_{\boldsymbol{IG}}|$. There are a large number of possible Λ sets. To keep the density real, we assume,

$$|\rho_{\boldsymbol{\Lambda}}(-\boldsymbol{q}_{\rm IG})|=|\rho_{\boldsymbol{\Lambda}}(\boldsymbol{q}_{\rm IG})|,\quad \delta_{{\rm IG},\boldsymbol{\Lambda}}(\boldsymbol{q}_{\rm IG})=-\,\delta_{{\rm IG},\boldsymbol{\Lambda}}(-\boldsymbol{q}_{\rm IG}). \tag{15}$$

The phase factor, $_{\rm IG,}(\boldsymbol{q}_{\rm IG})$, is added to avoid strong atom overlaps. To express the full density function, $\rho(\boldsymbol{r})$, we need to use the full spectrum of $\rho(\boldsymbol{q})$ as in equation (4). However, even with only one value of q with $q_{\rm IG}$ it is possible to reproduce the oscillations in $g(r)$, which becomes the MRO oscillation with an exponential damping as shown in figure 1. This is because the main oscillations in the MRO originate from the first peak of $S(q)$ [19, 20]. The first peak of $S(q)$ for the IG state is a δ-function. With the Lorentzian broadening, which produces the exponential decay in $g(r)$, it captures the first peak of $S(q)$ for real liquid. The high-q portion of $\rho(\boldsymbol{q})$ contributes chiefly to the first peak of $g(r)$ [19, 20]. Thus, it is evident that the minimum in $\phi_{pp}(q)$ provides the driving force toward the IG state and to increase the MRO coherence length, $\xi_{\rm s}$, with decreasing temperature following equation (3).

4. Scattering theory and the origin of the pseudopotential minimum

Another way to look at this result is from the viewpoint of the scattering theory. In the partial wave analysis of scattering [21] when a particle is scattered by a central symmetric potential, the incoming plane wave can be expanded into the Legendre polynomials, $P_\ell(\cos\theta)$, where θ is the angle between $\boldsymbol{q}$ and $\boldsymbol{r}$, as,

$$\psi(\boldsymbol{r}) = e^{iq\cdot r} = \sum_\ell (2\ell+1)\, i^\ell P_\ell(\cos\theta)\, J_\ell^0(qr). \tag{16}$$

where $J_\ell^m(z)$ is the spherical Bessel function. For the isotropic wave, $\ell = 0$,

$$J_0^0(z) = \frac{\sin z}{z}. \tag{17}$$

$J_0^0(z)$ has the first maximum at $z = 5\pi/2$. Therefore, the wave with $q_\mathrm{p} = 5\pi/2a$ is consistent with having the nearest neighbor atoms at $r = a$.

The expansion in equation (13) is the basis for the Fourier-transformation for a spherical potential in equation (8). Let us further break down $\phi_\mathrm{pp}(r)$ into the attractive part, $\phi_\mathrm{pp,att}(r)$, the negative portion of $\phi_\mathrm{pp}(r)$, for which $\phi_\mathrm{pp,att}(r) = 0$ below r_{c2} defined by $\phi_\mathrm{pp}(r_{c2}) = 0$, and the repulsive part $\phi_\mathrm{pp,rep}(r)$, the positive portion of $\phi_\mathrm{pp}(r)$, for which $\phi_\mathrm{pp,rep}(r) = 0$ above r_{c2} (figure 4). Then, for $\phi(r_\mathrm{c}) = 1$ eV ($r_\mathrm{c} = 2.22$ Å), the first maximum of $J_0^0(z)$ at $z = 5\pi/2$ produces a minimum in $\phi_\mathrm{pp,att}(q)$ at $Q = 2.82$ Å^{-1}, close to $q_\mathrm{att} = 5\pi/2r_\mathrm{min} = 3.00$ Å^{-1} as shown in figure 5. The actual minimum is a little less than q_att, most likely reflecting the asymmetry of $\phi_\mathrm{pp,att}(r)$. On the other hand, the first minimum of $J_0^0(z)$ at $3\pi/2$ results in a minimum of $\phi_\mathrm{pp,rep}(q)$ at 2.79 Å^{-1}, which is not far from $q_\mathrm{att} = 3.00$ Å^{-1}, as shown also in figure 5. Because the majority of interatomic distances fall in the range beyond r_{c2}, $\phi_\mathrm{pp,att}(r)$ is more important than $\phi_\mathrm{pp,rep}(r)$ in determining the structure. Thus, we may safely conclude that the primary driving force to form the density wave originates from the minimum in $\phi_\mathrm{pp,att}(q)$.

For the hard-sphere (HS) potential $\phi_\mathrm{pp,att}(r) = 0$, and $\phi_\mathrm{pp}(q) = \phi_\mathrm{pp,rep}(q)$. Indeed, the minimum appears at $qD = 1.85\pi$ where D is the HS radius [12], which is closer to $3\pi/2(= q_\mathrm{rep}D)$ than to $5\pi/2(= q_\mathrm{att}D)$. However, the HS system has no cohesion and is stabilized only by pressure which defines the density, whereas the effect of the pressure is not included in $\phi_\mathrm{pp}(q)$. At reasonable densities the average nearest neighbor distance, a, is significantly larger than D, making qa closer to $5\pi/2$. The HS model is widely used in soft-matter science, bolstered by the Weeks-Chandler-Andersen (WCA) rule for high temperature liquid [22]. However, it is questionable if the WCA principle still applies for supercooled liquid. The analysis above suggests that the stability of the density wave originates from the attractive part of the interatomic potential, and the repulsive part plays no or little role for supercooled liquid.

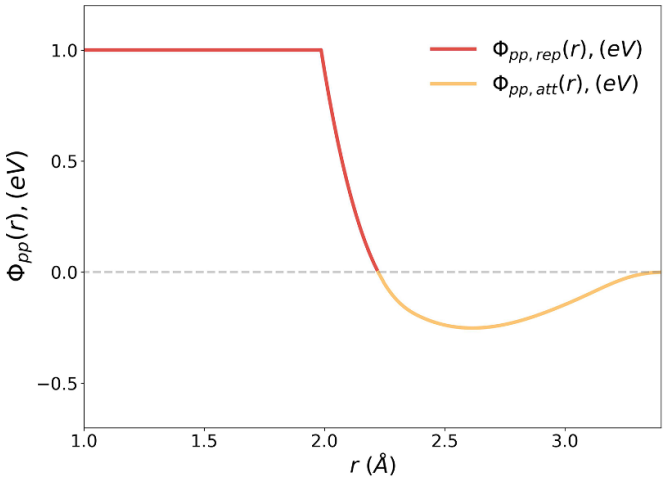

Figure 4. The repulsive part of $\phi_\mathrm{pp}(r)$, $\phi_\mathrm{pp,rep}(r)$, (dark color) and the attractive part of $\phi_\mathrm{pp}(r)$, $\phi_\mathrm{pp,att}(r)$ (light color).

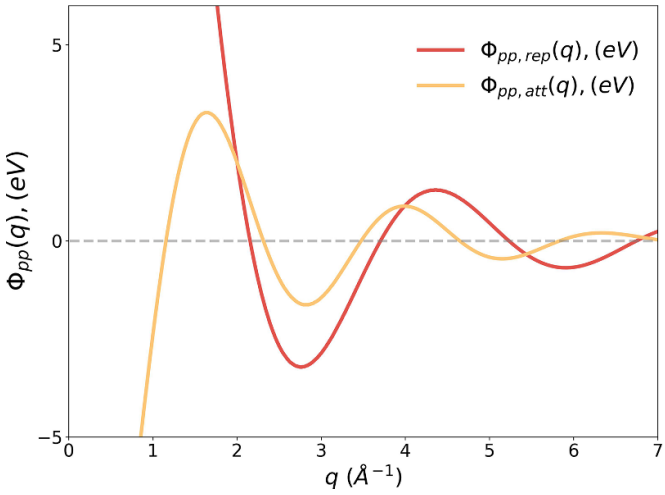

Figure 5. The repulsive part, $\phi_\mathrm{pp,rep}(q)$ (dark color) and the attractive part, $\phi_\mathrm{pp,att}(q)$ (light color).

5. Top–down vs. bottom–up

The IG state with long-range density waves, however, has a poor local structure. For instance, an icosahedral local cluster is a dominant topology in dense-random packed structure [4–7], but in the IG state its population is only 0.7% [9]. The first peak of $g(r)$, which describes the SRO, depends mainly on the high-q portion of $S(q)$, thus $\rho(q)$ which is not included in forming the IG density wave state. Therefore, the top–down approach to create the structure with the density wave state is in conflict with the bottom–up approach starting with the local SRO, and the MRO emerges as a compromise between the two [12, 13]. The value of ξ_s expresses the extent of the compromise. When the density waves dominate ξ_s is long, whereas it is short when the SRO wins. Therefore, ξ_s tends to be short for systems with strong covalent bonds which exert strong constraints on the SRO, and long for systems with metallic bonds which are more flexible with respect to disorder [23].

We define 'ideality' of the structure with the height of the first peak of $S(q)$ [20], thus the value of ξ_s [24]. The ideality is unrelated to chemical disorder, such as the atomic size incompatibility [20]. In certain oxide glasses increasing chemical complexity actually improves ideality by suppressing the effect of covalency [25]. This is a case of 'order out of disorder'.

In the conventional bottom–up approach, the MRO is just a consequence of the SRO [1–3, 14]. However, it is difficult to explain with the bottom–up approach why well-defined MRO is observed up to high temperatures even in chemically complex liquid [9, 20]. The dual approach including the top–down approach shows that a separate driving force exists to create the MRO to minimize the pseudopotential through the density waves, and explains well why the MRO is prevalent and becomes more extended with decreasing temperature, culminating with the glass transition.

6. Mechanical properties and defects

It was found that the MRO coherence length plays a major role in controlling the mechanical response of liquid. For instance, it is directly related to liquid fragility [26] through $\xi_s \sim m^3$, where m is the fragility coefficient [24]. Furthermore, the activation energy for viscosity, E_a, is proportional to the coherence volume, ${\xi_s}^3$, just above T_g [9]. At higher temperatures the power d for $E_a \sim {\xi_s}^d$ decreases with increasing temperature, from three at T_g down to zero at T_A [27]. These results suggest that the MRO, to be specific the resistance to shear stress by the density wave, controls the mechanical response. This view is consistent with the growing evidence that mechanical response of liquid and glass is controlled by correlations with a length-scale larger than the interatomic distance, rather than the nearest neighbor shell [15, 28–32].

On the other hand, this view is at odds with the more conventional view that the SRO determines mechanical response [33–37]. In the conventional view, the rigidity, or lack thereof, of the nearest neighbor cage controls atomic mobility through local jamming. However, the SRO does not freeze at the glass transition [11], retains some liquid-like population [38], and the nearest neighbor atoms become rearranged under applied shear stress [39, 40]. Therefore, the nearest neighbor shell is not quite rigid even in the glassy state, at least for a significant number of atoms. Instead, it is more likely that the resistance to flow is provided by the MRO, not by the SRO.

The conventional view also assumes that mechanical deformation occurs at structural defects, usually defined as soft spots, specified by local density or other parameters associated with the nearest neighbor shell [33–37, 41, 42]. This view needs to be questioned because,

1. The nearest neighbor atoms are rearranged by applied stress even before yielding [39, 40], and the initial state is altered.
2. After passing through the saddle point in the potential energy landscape (PEL) [43] the thermal memory is lost [44, 45], because the saddle point is a generator of chaos [46, 47].
3. The nearest neighbor shell is often loose and may not provide sufficient resistance to flow.

Thus, it is possible that the real resistance to deformation is provided by the MRO rather than the SRO. Structural defects may start local deformation, but the local structure keeps changing during deformation. By the time the system reaches the saddle point of the PEL it may not matter where deformation started because the thermal memory is largely lost. This subject, however, needs further study.

7. Conclusion

The MRO, represented by the oscillations in the PDF beyond the first peak, has not received sufficient attention it deserves, because it was considered to be a mere consequence of the SRO in the nearest neighbor shell. However, the density wave theory with the pseudopotential suggests that there is a separate driving force to create the density waves, which competes against the SRO and results in the MRO as a product of compromise. This balanced view, with the top–down (density wave) and bottom–up (SRO) approaches, explains a number of salient features of liquid and glass, and provides the basis for an alternative framework for the theory of liquid and glass.

Data availability statement

All data that support the findings of this study are included within the article (and any supplementary files).

Acknowledgments

This work was supported by the U. S. Department of Energy, Office of Science, Basic Energy Sciences, Materials Sciences and Engineering Division.

ORCID iDs

Takeshi Egami https://orcid.org/0000-0002-1126-0276
Chae Woo Ryu https://orcid.org/0000-0003-1588-4868

References

[1] Egelstaff P A 1967 *An Introduction to the Liquid State* 1st edn (London: Academic)
Egelstaff P A 1991 An Introduction to the *Liquid State* 2nd edn (Oxford: Oxford University Press)
[2] Croxton C A 1974 *Liquid State Physics—A Statistical Mechanical Introduction* (Cambridge: Cambridge University Press)
[3] Hansen J-P and McDonald I R 1976 *Theory of Simple Liquids* 1st edn (London: Academic)
Hansen J-P and McDonald I R 1986 *Theory of Simple Liquids* 2nd edn (London: Academic)
Hansen J-P and McDonald I R 2006 *Theory of Simple Liquids* 3rd edn (London: Academic)

[4] Bernal J D 1959 *Nature* **183** 141
[5] Nelson D R 1983 *Phys. Rev.* B **28** 5515
[6] Miracle D B 2004 *Nat. Mater.* **3** 697
[7] Sheng H W, Luo W K, Alamgir F M, Bai J M and Ma E 2006 *Nature* **439** 419
[8] Wu B, Iwashita T and Egami T 2018 *Phys. Rev. Lett.* **120** 135502
[9] Ryu C W, Dmowski W, Kelton K F, Lee G W, Park E S, Morris J R and Egami T 2019 *Sci. Rep.* **9** 18579
[10] Egami T 2020 *Front. Phys.* **8** 50
[11] Ryu C W and Egami T 2021 *Phys. Rev.* E **104** 064109
[12] Egami T and Ryu C W 2022 *Front. Mater.* **9** 874191
[13] Egami T and Ryu C W 2022 arXiv:2211.07702
[14] Ornstein L S and Zernike F 1914 *R. Neth., Acad. Arts Sci.* **17** 793
[15] Berthier L and Kob W 2012 *Phys. Rev.* E **85** 011102
[16] Alexander S and McTague J P 1978 *Phys. Rev. Lett.* **41** 702
[17] Sachdev S and Nelson D R 1985 *Phys. Rev.* B **32** 4592
[18] Srolovitz D, Maeda K, Vitek V and Egami T 1981 *Philos. Mag.* A **44** 847
[19] Cargill III G S 1975 *Solid State Phys.* **30** 227
[20] Ryu C W, Dmowski W and Egami T 2020 *Phys. Rev.* E **101** 030601(R)
[21] Wu T Y and Ohmura T 1962 *Quantum Theory of Scattering* (Englewood Cliffs, NJ: Prentice-Hall)
[22] Weeks J D, Chandler D and Andersen H C 1971 *J. Chem. Phys.* **54** 5237
[23] Egami T and Ryu C W 2021 *Phys. Rev.* E **104** 064110
[24] Ryu C W and Egami T 2020 *Phys. Rev.* E **102** 042615
[25] Westover A S *et al* 2023 *Chem. Mater.* accepted
[26] Angell C A 1995 *Science* **267** 1924
[27] Egami T and Ryu C W 2020 *Front. Chem.* **8** 579169
[28] Berthier L, Biroli G, Bouchaud J-P, Cipelletti L, El Masri D, L'Hôte D, Ladieu F and Pierno M 2005 *Science* **310** 1797
[29] Biroli G, Bouchaud J-P, Cavagna A, Grigera T S and Verrocchio P 2008 *Nat. Phys.* **4** 771
[30] Kob W, Roldan-Vargas S and Berthier L 2012 *Nat. Phys.* **8** 164
[31] Kob W and Berthier L 2013 *Phys. Rev. Lett.* **110** 245702
[32] Hocky G M, Berthier L, Kob W and Reichman D R 2014 *Phys. Rev.* E **89** 052311
[33] Spaepen F 1975 *Acta Metall.* **23** 615
[34] Argon A S 1979 *Acta Metall.* **27** 47
[35] Srolovitz D, Vitek V and Egami T 1983 *Acta Metall. Mater.* **31** 335
[36] Falk M L and Langer J S 1998 *Phys. Rev.* E **57** 7192
[37] Ding J, Cheng Y Q, Sheng H, Asta M, Ritchie R O and Ma E 2016 *Nat. Commun.* **7** 13733
[38] Egami T, Poon S J, Zhang Z and Keppens V 2007 *Phys. Rev.* B **76** 024203
[39] Dmowski W, Iwashita T, Chuang C-P, Almer J and Egami T 2020 *Phys. Rev. Lett.* **105** 205502
[40] Wang H, Dmowski W, Wang Z, Tong Y, Yokoyama Y, Ketkaew J, Schroers J and Egami T 2022 *Phys. Rev. Lett.* **128** 155501
[41] Cubuk E D, Schoenholz S S, Rieser J M, Malone B D, Rottler J, Durian D J, Kaxiras E and Liu A J 2015 *Phys. Rev. Lett.* **114** 108001
[42] Bapst V *et al* 2020 *Nat. Phys.* **16** 448
[43] Debenedetti P G and Stillinger F H 2001 *Nature* **410** 259
[44] Fan Y, Iwashita T and Egami T 2017 *Nat. Commun.* **8** 15417
[45] Ding J, Li L, Wang N, Tian L, Asta M, Ritchie R O and Egami T 2021 *Mater. Today Phys.* **17** 100359
[46] Mason J F and Piiroinen P T 2012 *Chaos* **22** 013106
[47] Párraga H, Arranz F J, Benito R M and Borondo F 2018 *J. Phys. Chem.* A **122** 3433